AAS 16-515

DYNAMIC OBSERVABILITY ANALYSIS FOR ATTITUDE, ANGULAR VELOCITY, SHAPE, AND SURFACE PARAMETERS

Richard Linares*
University of Minnesota, Twin City Campus, Minneapolis, NM, 55403
John L. Crassidis†
University at Buffalo, State University of New York, Amherst, NY, 14260-4400

This paper discusses a dynamic observability analysis for attitude, angular velocity, shape, and surface parameters of Space Objects (SOs) using non-resolved images or light curve measurements. The Fisher information matrix and Cramér-Rao lower bound are introduced for calculating the observability of parameters used in SO models. Light curve measurements are known to be functions of SO rotational states, shape geometry, and surface parameters. This dependency is captured in the bidirectional reflectance distribution functions models. The rotational dynamics of SOs can be difficult to model due to the fact that external and/or control torques are unknown. This work assumes that these torques are known, and under this assumption dynamic observability is analyzed. An illustrative two-dimensional example is considered. This example consists of a simplified system with one angle and one angle rate to model the rotational dynamics of the SO. The Cramér-Rao lower bound is used to study the effects of geometry on estimation performance. It was found that as the number of sides increases, and the SO shape tends to an axially symmetric one, the observability in the attitude estimates are lost. Finally, the Cramér-Rao lower bound is compared with actual performances from estimation approaches for estimating the attitude of an SO.

INTRODUCTION

Space Situational Awareness (SSA) is concerned with collecting and maintaining knowledge of all objects orbiting the Earth. The U.S. Air Force collects the necessary data for space object catalog development and maintenance through a global network of radars and optical sensors. Some of these sensors are powerful ground-based telescopes that can resolve large Space Objects (SOs) in Low Earth Orbits (LEOs) such as the Hubble Space Telescope and the International Space Station to high detail. Unfortunately, most objects are too small and/or too distant to lend themselves to ground-based resolved imaging; such classes of objects are labeled as "unresolved objects." In particular, SOs in Geosynchronous Orbits (GEOs), "micro" and "nano" satellites are too small to be resolved using ground-based optical telescopes, and fall under the class of unresolved objects. These unresolved objects are critical to SSA; they are important due to the threat they pose on active space objects, and characterizing them can be challenging.

In order to understand the nature and eventually the origin of these objects, physical characteristics such size, shape and material composition are required. These characteristics may be used

*Assistant Professor, Department of Aerospace Engineering and Mechanics. Email: rlinares@umn.edu, Member AIAA.
†CUBRC Professor in Space Situational Awareness, Department of Mechanical & Aerospace Engineering. Email: johnc@buffalo.edu, Fellow AIAA, Fellow AAS.

to provide identification attributes, and can also be obtained from existing data sources such as photometric and astrometric data.[?] To investigate the surface material properties reflectance spectroscopy data can be used.[?] Reflectance spectroscopy or multi-band photometric data can be used to study non-resolved debris objects and determine their material composition.[?] The measurements made of debris objects can be compared to laboratory derived measurements to determine material composition of the debris.[?,?,?]

Brightness is a function of the phase angle and can provide information on such things as: aging, material properties, shape classes, solar panel offsets and change analysis. For detailed surface material characterization, spectrometric and/or multi-band photometric measurements are generally required. Wavelength dependent photometric properties for materials, such as solar array panels, milled aluminum, anodized aluminum, multi-layer insulation and white paint, are available as part of the Time-domain Analysis Simulation for Advanced Tracking (TASAT)[?] signature simulation software package. Many of these show telltale signs of spectral features that can be used as fingerprints to identify the material composition of satellite surfaces in solar reflectance spectra. These spectral features will have the maximum observability at the glint configuration since glinting has very high magnitude spectral reflectance.

Optical signatures can be used to provide information about the SO. The phase angle is a variable of interest when reporting the brightness for SOs. The phase angle is the angle between the direction to the Sun and the direction to the observer, as seen at the object being observed. If the object is the Moon, a zero phase angle corresponds to a full Moon; at this angle the most light is reflected to the observer. Therefore when observing SOs, the maximum irradiance will occur at minimum phase angle. Non-resolved photometric data have been studied as a mechanism for space object characterization. Photometry is the measurement of an object's flux or apparent brightness measured over a wavelength band. The temporal variation of photometric measurements is referred to as photometric signature. The photometric optical signature of an object contains information about shape, attitude, size and material composition.[?,?,?,?,?] The goal of this paper is to use the Fisher Information Matrix and Cramér-Rao inequality to provide a lower bound on the expected estimation error for these quantities.

FISHER INFORMATION MATRIX

The Cramér-Rao inequality provides a lower bound on the expected error between an estimated quantity and the true quantity. The Cramér-Rao inequality is given by the following expression

$$P \equiv E\left\{\left(\hat{\mathbf{x}}-\mathbf{x}\right)\left(\hat{\mathbf{x}}-\mathbf{x}\right)^{T}\right\} \geq F^{-1} \tag{1}$$

where the matrix F is the Fisher Information Matrix (FIM) and $\hat{\mathbf{x}}$ is an estimate of the true value $\mathbf{x}$. The variable $\hat{\mathbf{x}}$ is a random variable with probability distribution function (pdf) $p(\hat{\mathbf{x}})$. The $E\{\cdot\}$ operator is the expectation of the argument with respect to the pdf $p(\hat{\mathbf{x}})$, where this expectation for continuous variables can be written as

$$E\left\{\mathbf{g}(\mathbf{x})\right\} = \int_{-\infty}^{\infty} \mathbf{g}(\mathbf{x}) p(\mathbf{x}) d\mathbf{x} \tag{2}$$

The likelihood function, $p(\tilde{\mathbf{y}}|\mathbf{x})$, of the measurement $\tilde{\mathbf{y}}$ given $\mathbf{x}$ for the Fisher information matrix is given by

$$F = E\left\{\left[\frac{\partial}{\partial \mathbf{x}} \log p(\tilde{\mathbf{y}}|\mathbf{x})\right]\left[\frac{\partial}{\partial \mathbf{x}} \log p(\tilde{\mathbf{y}}|\mathbf{x})\right]^{T}\right\} \tag{3}$$

The FIM can also be computed using the Hessian of the negative log likelihood function, given by

$$F = E\left\{\frac{\partial^2}{\partial \mathbf{x}\partial \mathbf{x}^T} L(\hat{\mathbf{y}}|\mathbf{x})\right\} \tag{4}$$

where $L(\tilde{\mathbf{y}}|\mathbf{x}) = -\log\{p(\tilde{\mathbf{y}}|\mathbf{x})\}$. If the measurement likelihood is a Gaussian distribution and the measurement relationship is given by $\tilde{\mathbf{y}} = \mathbf{h}(\mathbf{x}) + \mathbf{v}$, where $\mathbf{v}$ is measurement noise, which is assumed to be zero-mean with covariance R, then $L(\tilde{\mathbf{y}}|\mathbf{x})$ becomes

$$L(\tilde{\mathbf{y}}|\mathbf{x}) = \frac{1}{2}\left[\tilde{\mathbf{y}} - \mathbf{h}(\mathbf{x})\right] R^{-1} \left[\tilde{\mathbf{y}} - \mathbf{h}(\mathbf{x})\right]^T \tag{5}$$

Then the FIM is calculated from Equation (**??**):

$$F = E\left\{\frac{\partial^2}{\partial \mathbf{x}\partial \mathbf{x}^T} L(\hat{\mathbf{y}}|\mathbf{x})\right\} = E\left\{\frac{\partial h(\mathbf{x})}{\partial \mathbf{x}} R^{-1} \frac{\partial h(\mathbf{x})}{\partial \mathbf{x}}^T\right\} \tag{6}$$

If the pdf $p(\tilde{\mathbf{x}})$ is assumed to be Gaussian then the expression from Equation (**??**) is given by

$$F = \left.\frac{\partial h(\mathbf{x})}{\partial \mathbf{x}} R^{-1} \frac{\partial h(\mathbf{x})}{\partial \mathbf{x}}^T\right|_{\mathbf{x}=\mathbf{x}_{\text{true}}} \tag{7}$$

So far this model assumes one measurement vector but this can be extended to multiple vector measurements of the variable $\mathbf{x}$ denoted by $\mathbf{Y} = [\tilde{\mathbf{y}}_1, ..., \tilde{\mathbf{y}}_m]$. Then the observation function might be different for each measurement giving the following relationship:

$$\tilde{\mathbf{y}}_k = \mathbf{h}_k(\mathbf{x}) + \mathbf{v}_k \qquad k = 1, \ldots, m \tag{8}$$

where $\mathbf{v}_k$ is still a zero-mean Gaussian noise process. This model can represent measuring the same state vector at different time steps and therefore the index k can represent a time index assuming $\mathbf{x}$ is constant over time. Measurements might be correlated in this case, and thus we can write a collective measurement noise vector $\mathbf{V} = [\mathbf{v}_1, \ldots, \mathbf{v}_m]^T$ with covariance $\bar{R} = E\left\{\mathbf{V}\mathbf{V}^T\right\}$. If the measurements are correlated the Fisher information matrix is given by

$$F = \left.\frac{\partial \bar{\mathbf{h}}_k(\mathbf{x})}{\partial \mathbf{x}} \bar{R}_k^{-1} \frac{\partial \bar{\mathbf{h}}_k(\mathbf{x})}{\partial \mathbf{x}}^T\right|_{\mathbf{x}=\mathbf{x}_{\text{true}}} \tag{9}$$

where $\bar{\mathbf{h}}_k(\mathbf{x}) = [\mathbf{h}_1(\mathbf{x}), \ldots, \mathbf{h}_m(\mathbf{x})]^T$, and if the measurements are not correlated the FIM is given by

$$F = \left.\sum_{i=1}^{m} \frac{\partial \mathbf{h}_i(\mathbf{x})}{\partial \mathbf{x}} R_i^{-1} \frac{\partial \mathbf{h}_i(\mathbf{x})}{\partial \mathbf{x}}^T\right|_{\mathbf{x}=\mathbf{x}_{\text{true}}} \tag{10}$$

Now we assume that the true state $\mathbf{x}$ is time varying and follows the following ordinary differential equation:

$$\dot{\mathbf{x}} = \mathbf{f}(\mathbf{x}, t) \tag{11}$$

The solution flow in terms of the initial condition can be written as $\mathbf{x}(t_k) = \boldsymbol{\phi}(\mathbf{x}_0, t_k, t_0)$. Then for the case of a time-varying state the measurement function can be written as

$$\tilde{\mathbf{y}}\left(t_k\right) = \mathbf{h}\left(\boldsymbol{\phi}(\mathbf{x}_0, t_k, t_0)\right) + \mathbf{v}(t_k) \qquad t_k = t_1, \ldots, t_m \tag{12}$$

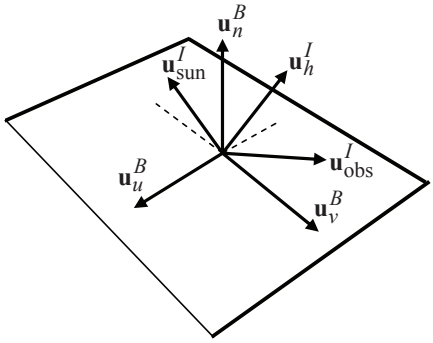

Figure 1. Reflection Geometry

Then the FIM can be written as[?]

$$F = \sum_{i=1}^{m} \Phi(t_k, t_0) \frac{\partial \mathbf{h}(\boldsymbol{\phi})}{\partial \boldsymbol{\phi}} R_k^{-1} \left(\Phi(t_k, t_0) \frac{\partial \mathbf{h}(\boldsymbol{\phi})}{\partial \boldsymbol{\phi}} \right)^T \Bigg|_{\mathbf{x}=\mathbf{x}_{0\text{true}}} \tag{13}$$

where the function $\frac{\partial \boldsymbol{\phi}}{\partial \mathbf{x}_0}$ is often referred to as the state transition matrix and can be written as $\Phi(t_k, t_0) \equiv \frac{\partial \boldsymbol{\phi}}{\partial \mathbf{x}_0}$. Finally for this nonlinear dynamical system the Cramér-Rao lower bound (CRLB) covariance is given by

$$P = \left(\sum_{i=1}^{m} F_i \right)^{-1} \tag{14}$$

where the F_i are the individual FIM for each measurement. Using the F_i can give us an indication of the information that a measurement contributes to each state. The F_i matrix may not be full rank but it can still be used to study the information geometry of the system for an individual measurement or a sequence of measurements by studying the eigen-structure of F_i. We also consider parametric states in this analysis.

Review of Bidirectional Distribution Functions

A number of bidirectional reflectance distribution functions (BRDFs) exist in the literature. These models are based on the BRDF that models light distribution scattered from the surface due to the incident light. The BRDF at any point on the surface is a function of two directions, the direction from which the light source originates and the direction from which the scattered light leaves the observed the surface. These models include Ashikhmin-Shirley,[?] a simplified Blinn-Phong,[?] and Cook-Torrance[?] to list some. The BRDF models how light energy reflects off of surfaces and how this reflected energy is distributed in varios directions. The brightness of an object in space can be modeled using an anisotropic Phong light diffusion model.[?]

The model in Ref. **?** decomposes the BRDF into a specular component and a diffuse component. The two terms sum to give the total BRDF:

$$\rho_{\text{total}}(i) = \rho_{\text{spec}}(i) + \rho_{\text{diff}}(i) \tag{15}$$

The diffuse component represents light that is scattered equally in all directions (Lambertian) and the specular component represents light that is concentrated about some direction (mirror-like).

Reference **?** develops a model for continuous arbitrary surfaces but simplifies for flat surfaces. This simplified model is employed in this work as shape models are considered to consist of a finite number of flat facets. Therefore the total observed brightness of an object becomes the sum of the contribution from each facet:

$$f_r = (dR_d + sR_s) \tag{16}$$

which depends on the diffuse bidirectional reflectance (R_d), the specular bidirectional reflectance (R_s), and the fraction of each to the total (d and s respectively where $d+s=1$). These bidirectional reflectances are calculated differently for the various models. In each model, however, $c = \mathbf{u}_{\text{obs}}^{I\ T}\mathbf{u}_h^I$ (geometry shown in Figure **??**), ρ is the diffuse reflectance ($0 \leq \rho \leq 1$), and F_0 is the specular reflectance of the surface at normal incidence ($0 \leq F_0 \leq 1$). To be used as a prediction tool for brightness and radiation pressure calculations, an important aspect of the BRDF is energy conservation. For energy to be conserved, the integral of the BRDF times $\cos(\theta_r)$ over all solid angles in the hemisphere with $\theta_r \leq 90$ needs to be less than unity, with

$$\int_0^{2\pi}\int_0^{\pi/2} f_r \cos(\theta_r)\sin(\theta_r)\, d\theta_r d\phi = R_d + R_s \tag{17}$$

For the BRDF given in Eq. (**??**), this corresponds to constant values of $R_d = d\rho$ and $R_s = sF_0$. The remaining energy not reflected by the surface is either transmitted or absorbed. In this paper it is assumed the transmitted energy is zero. A review of the various BRDS functions is provided in Table **??**.

Ashikhmin-Shirley BRDF: In addition to d, ρ, and F_0, the Ashikhmin-Shirley BRDF has two exponential factors (n_u, n_v) that define the reflectance properties of each surface. The Ashikhmin-Shirley diffuse and specular reflectivities are not constant, however, but rather complicated functions of illumination angle, exponential factor, and the diffuse and specular reflectances. In all cases, however, $R_d + R_s \leq 1$, so energy is conserved.

Blinn-Phong: The specular bidirectional reflectance of the original Phong model is proportional to $\left(\mathbf{u}_n^{I\ T}(i)\mathbf{R}\right)^n$, where $\mathbf{R}$ is the perfect mirror-like reflection of $\mathbf{u}_{\text{sun}}^{I\ T}$. Blinn**?** proposes that $\mathbf{u}_h^I$ be used instead of $\mathbf{R}$ to make it easier and faster to calculate. Unfortunately, both versions of the model do not conserve energy and thus are unsuited for the purposes of brightness estimation. The model can be made to conserve energy, however, by modifying the leading term. In keeping with the desire for simplicity in this model, the leading term is chosen to only be a function of the exponential factor and set to yield a reflectivity equal to the mirror-like reflection of Eq. (3) at normal illumination. In addition to d, ρ and F_0, the simplified Blinn-Phong BRDF has a single exponential factor (n) that defines the reflectance properties of each surface.

Cook-Torrance BRDF: This model has the facet slope distribution function (D), the geometrical attenuation factor (G) and the reflectance of a perfectly smooth surface (F) with $g = n^2 + c^2 - 1$ and the index of refraction $n = \frac{1+\sqrt{F_0}}{1-\sqrt{F_0}}$. In addition to d, ρ, and F_0, the Cook-Torrance BRDF has a facet slope (m) parameter that defines the reflectance properties of each surface. The facet slope parameter of the Cook-Torrance BRDF and the exponential factor of the Ashikhmin-Shirley and Blinn-Phong BRDFs are roughly related by $n = 2/m^2$.

Table 1. Review of Bidirectional Distribution Functions

Lambertian	$R_d = \frac{\rho d}{\pi}$ $R_s = 0$
non-Lambertian diffuse	$R_s = 0$ $R_d = F_0 \left(1 - \left(1 - \mathbf{u}_n^{I\,T}(i)\mathbf{u}_{\text{sun}}^I/2\right)^5\right)\left(1 - \left(1 - \mathbf{u}_n^{I\,T}(i)\mathbf{u}_{\text{obs}}^I/2\right)^5\right)$
Ashikhmin-Shirley	$F = F_0 + \left(\frac{1}{s} - F_0\right)(1-c)^5$ $R_d = \frac{28\rho}{23\pi}(1 - sF_0)\left(1 - \left(1 - \frac{\mathbf{u}_n^{I\,T}(i)\mathbf{u}_{\text{sun}}^I}{2}\right)^5\right)\left(1 - \left(1 - \frac{\mathbf{u}_n^{I\,T}(i)\mathbf{u}_{\text{obs}}^I}{2}\right)^5\right)$ $R_s = \frac{\sqrt{(n_u+1)(n_v+1)}}{8\pi}\frac{F}{c\max\left[\mathbf{u}_n^{I\,T}(i)\mathbf{u}_{\text{sun}}^I, \mathbf{u}_n^I(i)\mathbf{u}_{\text{obs}}^I\right]}(\cos(\alpha))^{n_u\cos^2(\beta)+n_v\sin^2(\beta)}$
Cook-Torrance	$R_d = \rho/\pi$ $D = \frac{1}{\pi m^2\cos^4\alpha}e^{\tan(\alpha)/m^2}$ $G = \min\left\{1, \frac{2\left(\mathbf{u}_n^{I\,T}(i)\mathbf{H}\right)\left(\mathbf{u}_n^{I\,T}(i)\mathbf{u}_{\text{obs}}^I\right)}{\mathbf{u}_{\text{obs}}^{I\,T}\mathbf{H}}, \frac{2\left(\mathbf{u}_n^{I\,T}(i)\mathbf{u}_{\text{sun}}^{I\,T}\right)\left(\mathbf{u}_n^{I\,T}(i)\mathbf{H}\right)}{\mathbf{u}_{\text{obs}}^{I\,T}\mathbf{H}}\right\}$ $F = \frac{(g-c)^2}{2(g+c)^2}\left\{1 + \frac{[c(g+c)-1]^2}{[c(g-c)+1]^2}\right\}$ $R_s = \frac{DGF}{4\left(\mathbf{u}_n^{I\,T}(i)\mathbf{u}_{\text{sun}}^I\right)\left(\mathbf{u}_n^{I\,T}(i)\mathbf{u}_{\text{obs}}^I\right)}$
Blinn-Phong	$R_d = \frac{\rho d}{\pi}$ $R_s = (1-d)\left(\frac{F_0(n+2)(n+4)}{8\pi(n+2^{-n/2})}\right)\left(\mathbf{u}_n^{I\,T}(i)\mathbf{u}_h^I\right)$

Light Curve Model Partial Calculation

In this section the partials of the light curve model with respect dynamic and parametric states are calculated. The state vector can be written as

$$\mathbf{x}^T = [\mathcal{P}(1)^T \ \ldots \ \mathcal{P}(N_F)^T \quad \mathcal{S}(1)^T \ \ldots \ \mathcal{S}(N_F)^T \quad \mathcal{D}^T \quad \mathcal{O}^T] \tag{18}$$

where $\mathcal{P}$, $\mathcal{S}$, $\mathcal{D}$, and $\mathcal{O}$ represent the shape, surface scattering, rotational and orbital parameters, respectively. The relevant parameters that go into these sets are defined by $\mathcal{P}(i) = [\mathcal{A}(i) \quad \phi(i) \quad g(i)]^T$, $\mathcal{S}(i)^T = [R_{\text{spec}}(i)^T \quad R_{\text{diff}}(i)^T \quad n_u(i) \quad n_v(i)]$, $\mathcal{D}^T = [\mathbf{q}_I^{B\,T} \quad \boldsymbol{\omega}_{B/I}^{B\,T}]$, and $\mathcal{O}^T = [\mathbf{r}^{I^T} \quad \mathbf{v}^{I^T}]$. Here it is assumed the arrangement of the facets and their normal vectors is known, and therefore only $\mathcal{A}(i)$ is needed to describe the shape. The following notation is used to represent partial of each parameter set with respect to the state vector:

$$\frac{\partial \mathbf{x}}{\partial \mathcal{S}} = \begin{bmatrix} 0_{3\times 3} & I_{3\times 3} & 0_{3\times(n-6)} \end{bmatrix} \tag{19}$$

where similar expressions are written for $\mathcal{P}$, $\mathcal{D}$, and $\mathcal{O}$, where n denotes the size of the state vector. The number of parameters depends on modeling of the SOs, mainly the number sides, and relevant parameters used in the light curve model. The parameters used for shape and the light curve model

might change based on application, and therefore there are many choices for these parameters. This work focuses on the Ashikhmin-Shirley model.

Typically, small Euler angles are used to parameterize the attitude matrix when preforming error analysis. The attitude linearization has been shown to be valid for the case of small attitude errors,[?] which is also assumed here. The noise linearization will produce an accurate covariance expression for large signal-to-noise ratios; even with errors of 1 degree this is not a concern.[?] The attitude matrix can be parameterized by vector of angle errors, $\boldsymbol{\delta\alpha}$, mapping the true attitude to the estimated attitude:

$$\hat{A} = \exp\left\{-[\boldsymbol{\delta\alpha}\times]\right\} A_{\text{true}} \tag{20}$$

The matrix exponential can be expanded in a Taylor series

$$\exp\left\{-[\boldsymbol{\delta\alpha}\times]\right\} = \sum_{n=0}^{\infty} \frac{1}{n!} \left(-[\boldsymbol{\delta\alpha}\times]\right)^n \approx I_{3\times 3} - [\boldsymbol{\delta\alpha}\times] \tag{21}$$

Keeping only the first order term gives the following approximation:

$$\hat{A} = \exp\left\{-[\boldsymbol{\delta\alpha}\times]\right\} A_{\text{true}} \approx \left(I_{3\times 3} - [\boldsymbol{\delta\alpha}\times]\right) A_{\text{true}} \tag{22}$$

Substituting this approximation into $\mathbf{u}_n^I(i) = \hat{A}\mathbf{u}_n^B(i)$ gives

$$\mathbf{u}_n^I(i) = {A_{\text{true}}}^T \left(I_{3\times 3} + [\boldsymbol{\delta\alpha}\times]\right) \mathbf{u}_n^B(i) \tag{23}$$

The partial with respect to the state vector is then

$$\frac{\partial \mathbf{u}_n^I(i)}{\partial \mathbf{x}} = -{A_{\text{true}}}^T [\mathbf{u}_n^B(i)\times] \frac{\partial \boldsymbol{\delta\alpha}}{\partial \mathbf{x}} \tag{24}$$

The partial of the vector $\mathbf{u}_{\text{sun}}^I$ with respect to the state vector involves taking the partial with respect to the position vector. It is assumed that the position of the SO is known for this work, and therefore $\mathbf{u}_{\text{sun}}^I$ and $\mathbf{u}_{\text{obs}}^I$ are known. The magnitude function partial derivative with respect to the state variables can be written as the following:

$$\frac{\partial m_{\text{app}}}{\partial \mathbf{x}} = -\frac{2.5}{F_{\text{obs}} \ln(10)} \frac{\partial F_{\text{obs}}}{\partial \mathbf{x}} \tag{25}$$

Note that since one can use the flux directly as a measurement the term $\frac{\partial F}{\partial \mathbf{x}}$ might only represent the measurement function partial. The flux partial can be expanded for any of the light curve models discussed earlier, the final expressions will not be shown here but are shown in Ref. **?**. For illustrative purposes a simple light curve model can be analyzed assuming that the object consists of a collection of N facets with only diffuse reflection and a non-Lambertian BRDF model given in Table **??**. The energy flux as seen by an observer can be written as

$$f(\boldsymbol{\theta}, t) = \sum_{i=1}^{N} \frac{\Phi_{\text{sun,vis}}}{\pi r^2} \alpha_d(i) C \left(\mathbf{u}_{\text{sun}}^I(t)^T A(t) \mathbf{u}_n^B(i)\right) \left(\mathbf{u}_{\text{obs}}^I(t)^T A(t) \mathbf{u}_n^B(i)\right) \tag{26}$$

where

$$C = \left(1 - \left(1 - \mathbf{u}_{\text{sun}}^I(t)^T A(t) \mathbf{u}_n^B(i)/2\right)^5\right) \left(1 - \left(1 - \mathbf{u}_{\text{obs}}^I(t)^T A(t) \mathbf{u}_n^B(i)/2\right)^5\right) \tag{27}$$

Then under the faceted model assumption, and only considering diffusion reflection the albedo normalized shape of the SO can be described by the collection of $\alpha_d(i)$ and $\mathbf{u}_n^B(i)$. The unit vector, $\mathbf{u}_n^B(i)$, can parameterized with two angles ϕ_i and g_i. Then $\mathbf{u}_n^B(i)$ is given by

$$\mathbf{u}_n^B(i) = \begin{bmatrix} \cos(\phi_i)\sqrt{1-g_i^2} \\ \sin(\phi_i)\sqrt{1-g_i^2} \\ g_i \end{bmatrix} \tag{28}$$

Then the FIM can be calculated by

$$F(\boldsymbol{\theta}) = \frac{1}{\sigma_m^2}\sum_{i=1}^{m}\left[\frac{\partial}{\partial\boldsymbol{\theta}}f(\boldsymbol{\theta},t_i)\right]^T\left[\frac{\partial}{\partial\boldsymbol{\theta}}f(\boldsymbol{\theta},t_i)\right] \tag{29}$$

where the form of the FIM will depend on the contents of the state vector, $\boldsymbol{\theta}$, and the light curve model used. The partial derivatives of the simplified measurement function are calculated as

$$\frac{\partial}{\partial\boldsymbol{\theta}}f(\boldsymbol{\theta},t_i) = \left[\frac{\partial}{\partial\boldsymbol{\omega}}, \quad \frac{\partial}{\partial\alpha_d(1)}, \quad \frac{\partial}{\partial g_1}, \quad \frac{\partial}{\partial\phi_1}, \cdots, \frac{\partial}{\partial\alpha_d(N)}, \quad \frac{\partial}{\partial g_N}, \quad \frac{\partial}{\partial\phi_N}\right]^T f(\boldsymbol{\theta},t_i) \tag{30}$$

Then the rest of the partial derivatives are as follows:

$$\frac{\partial}{\partial\alpha_d(i)}f(\boldsymbol{\theta},t_i) = \frac{zq}{\pi}C \tag{31a}$$

$$\frac{\partial}{\partial\phi_i}f(\boldsymbol{\theta},t_i) = C_1\mathbf{u}_{\text{obs}}^I(t)\left[\frac{\partial}{\partial\phi_i}\mathbf{u}_n^B(i)\right] + C_2\mathbf{u}_{\text{sun}}^I(t)\left[\frac{\partial}{\partial\phi_i}\mathbf{u}_n^B(i)\right] \tag{31b}$$

$$\frac{\partial}{\partial g_i}f(\boldsymbol{\theta},t_i) = C_1\mathbf{u}_{\text{obs}}^I(t)\left[\frac{\partial}{\partial g_i}\mathbf{u}_n^B(i)\right] + C_2\mathbf{u}_{\text{sun}}^I(t)\left[\frac{\partial}{\partial g_i}\mathbf{u}_n^B(i)\right] \tag{31c}$$

$$C_1 = \frac{\alpha_d(i)}{\pi}\left[\frac{5}{2}zq\left(1-(1-z/2)^4\right)\left(1-(1-q/2)^5\right)+Cq\right] \tag{31d}$$

$$C_2 = \frac{\alpha_d(i)}{\pi}\left[\frac{5}{2}zq\left(1-(1-z/2)^5\right)\left(1-(1-q/2)^4\right)+Cz\right] \tag{31e}$$

$$\left[\frac{\partial}{\partial\phi_i}\mathbf{u}_n^B(i)\right] = \left[-g_i\sin(\phi_i)\sqrt{1-g_i^2}, \quad \cos(\phi_i)\sqrt{1-g_i^2}, \quad 0\right]^T \tag{31f}$$

$$\left[\frac{\partial}{\partial g_i}\mathbf{u}_n^B(i)\right] = \left[-g_i\cos(\phi_i)\left(1-g_i^2\right)^{-1/2}, \quad -g_i\sin(\phi_i)\left(1-g_i^2\right)^{-1/2}, \quad 1\right]^T \tag{31g}$$

where z and q are given by $q = \left(\mathbf{u}_{\text{sun}}^I(t)^T A(t)\mathbf{u}_n^B(i)\right)$ and $z = \left(\mathbf{u}_{\text{obs}}^I(t)^T A(t)\mathbf{u}_n^B(i)\right)$, respectively.

ROTATIONAL DYNAMICS

In terms of the quaternion, the attitude matrix is given by

$$A(\mathbf{q}) = \Xi^T(\mathbf{q})\Psi(\mathbf{q}) \tag{32}$$

where

$$\Xi(\mathbf{q}) \equiv \begin{bmatrix} q_4 I_{3\times3} + [\boldsymbol{\varrho}\times] \\ -\boldsymbol{\varrho}^T \end{bmatrix} \tag{33a}$$

$$\Psi(\mathbf{q}) \equiv \begin{bmatrix} q_4 I_{3\times3} - [\boldsymbol{\varrho}\times] \\ -\boldsymbol{\varrho}^T \end{bmatrix} \tag{33b}$$

with

$$[\mathbf{a}\times] \equiv \begin{bmatrix} 0 & -a_3 & a_2 \\ a_3 & 0 & -a_1 \\ -a_2 & a_1 & 0 \end{bmatrix} \tag{34}$$

for any general 3×1 vector $\mathbf{a}$ defined such that $[\mathbf{a}\times]\mathbf{b} = \mathbf{a} \times \mathbf{b}$. This representation is constrained since the quaternion is of unit length and therefore $\mathbf{q}^T\mathbf{q} = 1$. The kinematics dynamics are given by a first-order differential equation:

$$\dot{\mathbf{q}} = \frac{1}{2}\Xi(\mathbf{q})\boldsymbol{\omega} \tag{35a}$$

$$\dot{\boldsymbol{\omega}}^B_{B/I} = J_{\text{SO}}^{-1}\left(-\left[\boldsymbol{\omega}^B_{B/I}\times\right] J_{\text{SO}}\boldsymbol{\omega}^B_{B/I}\right) \tag{35b}$$

Then the rotational dynamics is linearized by considering first order terms and small angle approximation:[?]

$$\dot{\boldsymbol{\delta\alpha}} = -\left[\hat{\boldsymbol{\omega}}^B_{B/I}\times\right]\boldsymbol{\delta\alpha} + \boldsymbol{\omega}^B_{B/I} \tag{36a}$$

$$\dot{\boldsymbol{\omega}}^B_{B/I} = J_{\text{SO}}^{-1}\left(-\left[J_{\text{SO}}\hat{\boldsymbol{\omega}}^B_{B/I}\times\right] + \left[\hat{\boldsymbol{\omega}}^B_{B/I}\times\right] J_{\text{SO}}\right)\boldsymbol{\omega}^B_{B/I} \tag{36b}$$

where $\hat{\boldsymbol{\omega}}^B_{B/I}$ is the true angular velocity about which the equations are linearized. Using the linearized equations above the state transition matrix can be calculated for a time step of Δt using the matrix exponential. Then Eq. (**??**) can be written in state space form as

$$\begin{bmatrix} \boldsymbol{\delta\dot{\alpha}} \\ \dot{\boldsymbol{\omega}}^B_{B/I} \end{bmatrix} = \underbrace{\begin{bmatrix} -\left[\hat{\boldsymbol{\omega}}^B_{B/I}\times\right] & I_{3\times3} \\ 0_{3\times3} & \left(-\left[J_{\text{SO}}\hat{\boldsymbol{\omega}}^B_{B/I}\times\right] + \left[\hat{\boldsymbol{\omega}}^B_{B/I}\times\right] J_{\text{SO}}\right) \end{bmatrix}}_{F} \begin{bmatrix} \boldsymbol{\delta\alpha} \\ \boldsymbol{\omega}^B_{B/I} \end{bmatrix} \tag{37}$$

The dynamic equations are linearized at the time of each measurement, and the linear dynamic matrix, F, is used to calculate the state transition matrix between t_k and t_{k-1}. In general, F can be taken to be a time-varying form t_{k-1} to t_k but for this work it is approximated as constant since the time between measurements, Δt, is expected to be small. Then the state transition matrix for the dynamic state is given by

$$\Phi(t_k, t_{k-1}) = \exp\left\{F(t_{k-1})\Delta t\right\} \tag{38}$$

where $F(t_{k-1})$ is linearized about the time of the previous measurements and then state transition matrix given in Eq. (**??**) is calculated as

$$\Phi(t_k, t_0) = \prod_{i=1}^{k} \Phi(t_i, t_{i-1}) \tag{39}$$

Finally, the CRLB can be calculated using Eq. (**??**) and the light curve models discussed earlier.

OBSERVABILITY ANALYSIS FOR LIGHT CURVE MEASUREMENTS

Using light curves for satellite orientation and surface parameter estimation has many inherent challenges. This section studies this problem, and first presents a simplified state model to highlight some of these challenges. First a simple two-dimensional model with one orientation angle and

one angular rate state is shown. This simplified model is used to show the challenges that object symmetry poses specifically to the light curve process.

The benefit of studying this simplified system is that one can remove the nonlinearities from the dynamic equations, and therefore isolate the nonlinearity in the measurements equations, i.e. the light curve model. After the simplified cases are shown the same nonlinear estimation techniques are studied to process light curves for satellite orientation and surface parameter estimation. New challenges are present for the full-state model, including the many nonlinearities in the dynamic equations and high degree of freedom for the desired parameters.

Analysis of Lambertian Model

The Lambertian BRDF model, given in Table **??**, is a simple light curve model which only accounts for pure Lambertian reflection (equal reflection is all directions). The energy flux as seen by an observer given the Lambertian can be written as

$$f(\boldsymbol{\theta}, t_i) = \sum_{i=1}^{N} \frac{\Phi_{\text{sun,vis}}}{\pi r^2} \alpha_d(i) z(t_i) q(t_i) \tag{40}$$

Let us assume that the flux is normalized such that $y_i = f(\boldsymbol{\theta}, t_i)\pi r^2/\Phi_{\text{sun,vis}}$, and for simplicity let us consider a one facet model where $N = 1$ and $A = I_{3\times 3}$. If it is assumed that $\mathbf{u}^I_{\text{obs}} = \mathbf{u}^I_{\text{sun}}$ and $\mathbf{u}^I_{\text{obs}} = [1 \quad 0 \quad 0]^T$ then the relationship between $\alpha_d(i)$ and g can be analyzed. Under these assumptions the following relation exists: $q(t_i) = z(t_i)$, and if the angle ϕ is neglected the angle between $\mathbf{u}^I_{\text{obs}}$ and $\mathbf{u}^I_n(i)$ can be written as $\mathbf{u}^{I\,T}_n(i)\mathbf{u}^I_{\text{obs}} = \sqrt{1-g^2}$. Then the normalized flux y_i is given by

$$y_i = \alpha_d (\mathbf{u}^{I\,T}_n(i)\mathbf{u}^I_{\text{obs}})^2 \tag{41}$$

Note that $(\mathbf{u}^{I\,T}_n(i)\mathbf{u}^I_{\text{obs}})^2 = 1 - g^2$, and therefore a direct relationship between g and α_d can be determined:

$$\alpha_d = \frac{y_i}{1-g^2} \tag{42}$$

This relationship is surprisingly accurate, which can approximate the general trend between α_d and g for more complex models. The Lambertian term is included in all models, and therefore this relationship is seen in all models to some extent. In a similar manner relations between ϕ and α_d can be found given by $\alpha_d = \frac{y_i}{\cos^2(\phi)}$. Considering the effect of both parameters under these assumptions yeilds

$$\alpha_d = \frac{y_i}{\cos^2(\phi)\,(1-g^2)} \tag{43}$$

Figure **??** shows both of these relationships for $y_i = 1$. From the Figure it is clear that for a single measurement a facet of albedo areas given by Eq. (**??**) are all equally likely. To see the accuracy of these relationship for more complex models the likelihood function using a single pass observation geometry is considered. The geometry is such that $\mathbf{u}^{I\,T}_n(i)$ rotates on the x-y plane from the $-y$ direction to the $+y$ direction, and there is no motion in the z direction. The Sun direction is held constant at $\mathbf{u}^I_{\text{sun}} = [1 \quad 0 \quad 0]^T$.

Figures **??** and **??** show the loglog of the target density for a single pass. Figure **??** shows the target density in the θ-g space. From this figure it can be seen that the location of the facet is weakly observable in the direction perpendicular to the pass. The location has high variation in the g direction and smaller variation is the θ direction. Figure **??** shows the target density in the θ-a

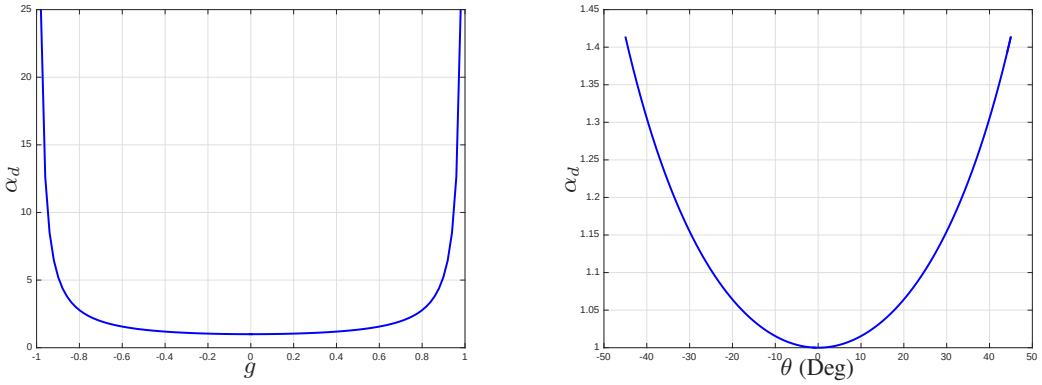

(a) Flux for Varying Number of Sides (b) Magnitude for Varying Number of Sides

Figure 2. Simple Lambertian Model Relationship

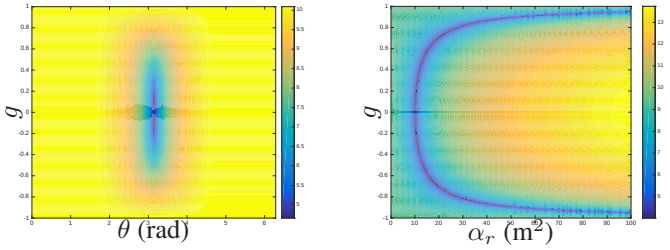

(a) Single Pass g vs. θ (b) Single Pass g vs. α_r

Figure 3. Contour of Likelihood Function

space. Here it is seen that the target density is highly non-Gaussian. From this figure it is clear that for a true location of $g = 0$, the measurement can be reproduced by a high value of g with a larger area. Increasing g results in a larger angle between the observer and the normal, but by increasing the area the effect of increasing this angle can be negated.

Simple Two-Dimensional State Model

To study the effects of shape on the resulting light curve, a simplified scenario is considered. Here, we consider prismatic shape models are consideredwith varying number of sides n, where $n \equiv N_F - 2$. The orientation of the models are such that the $\mathbf{B}_3$ direction is aligned with inertial $\hat{\mathbf{i}}_3$ axis, where $\{\hat{\mathbf{i}}_1, \hat{\mathbf{i}}_2, \hat{\mathbf{i}}_3\}$ defines the basis of the inertial reference frame. The models are allowed to rotate only about the $\mathbf{B}_3$ axis with the angle of rotation defined by θ. The rate of rotation is given by $\omega = \dot{\theta}$, and is assumed to be constant. Figure **??** shows the geometry of the simple test case. The Sun vector $\mathbf{u}^I_{\text{sun}}$ and observer direction vector $\mathbf{u}^I_{\text{obs}}$ are defined to lie in the $\hat{\mathbf{i}}_1 - \hat{\mathbf{i}}_2$ plane. The dynamic model is summarized as

$$\dot{\theta} = \omega \tag{44a}$$

$$\dot{\omega} = 0 \tag{44b}$$

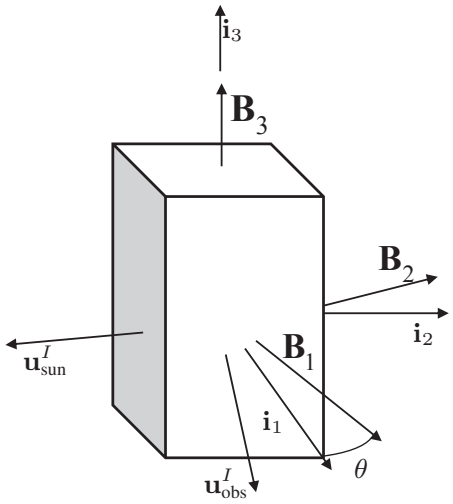

Figure 4. Test Case Definition

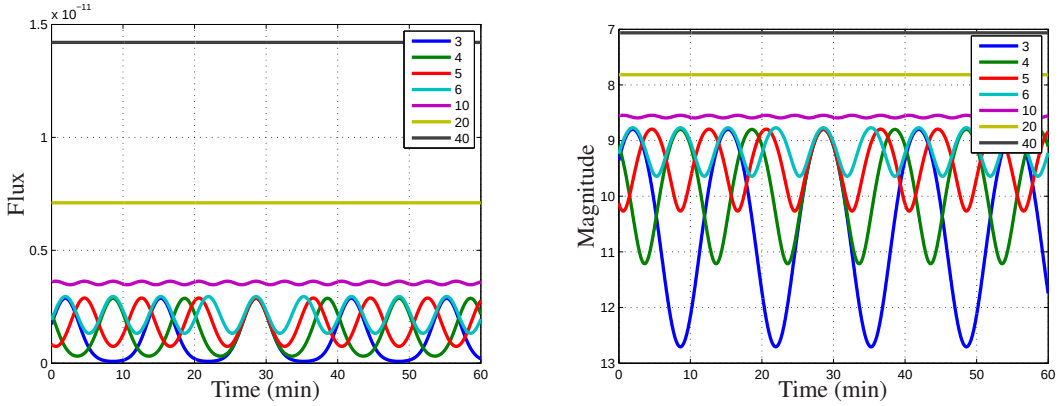

(a) Flux for Varying Number of Sides

(b) Magnitude for Varying Number of Sides

Figure 5. Flux and Magnitude for Varying Number of Sides

Then the system and measurement equations can be written in the following form:

$$\dot{\mathbf{x}} = F\mathbf{x} \tag{45a}$$

$$\tilde{\mathbf{y}} = \mathbf{h}\left(\mathbf{x}, \mathbf{p}\right) + \mathbf{v} \tag{45b}$$

where

$$F = \begin{bmatrix} 0 & 1 \\ 0 & 0 \end{bmatrix} \tag{46}$$

and $\mathbf{h}\left(\mathbf{x}, \mathbf{p}\right)$ is the nonlinear light curve measurement function. Here $\mathbf{p}$ is a vector of the light curve model parameter, such as shape and surface parameters. Then the state transition matrix for this simple example is given by Eq. (**??**).

Shape Geometry Effect

The shape model of the SO influences the attitude estimate and orientation parameter observability. For example axially symmetric bodies are expected to have no observability for the rotation

about the axis of symmetry, since reflection properties are invariant for rotation about this axis of symmetry. To study this effect, the number of sides n is varied, $n \in \{3,\ 4,\ 5,\ 6,\ 10,\ 20,\ 40\}$. The simulated light curves can be seen in Figure **??**. Figures **??** and **??** show the true flux and magnitude respectively. From these figures one can see that as the number of sides increases the light curves increase in frequency and are modulated. This effect also highlights the fact that for a given light curve the number of sides cannot be confused with the angular frequency since as the sides increase the brightness flotation magnitude is decreased or modulated. One can also see that the fluctuations are smaller but the mean signal increases. This is due to the fact that as the number of sides increases more sides tend to contribute to the brightness at a given orientation and therefore increases the overall brightness. Also, since the fluctuation becomes smaller it is more difficult to estimate the attitude since the signal-to-noise ratio of the fluctuations is low. Clearly, then as $n \to \infty$ the faceted regular prism model becomes a cylinder, at which point the attitude becomes unobservable due to axial symmetry about the axis of rotation.

To further investigate the effect of geometry, an observability study is conducted using the Cramér-Rao lower bound shown in Eq. (**??**). The Fisher information matrix is calculated from Eq. (**??**), and then the covariance is computed from the CRLB for each case by $P = F^{-1}$. In each case, an initial covariance is set to 25 degs for the attitude angle and 1500 deg/hr for the angular velocity. The partial derivative of the light curve model is computed using the equations discussed earlier. Figure **??** shows the attitude estimation CRLB obtained from the light curve data from Figure **??**. It is clearly seen that the estimator takes longer to converge for larger values of n consistent with diminishing observability. This analysis shows that as objects tend to smoother shapes with more symmetry attitude estimation observability is lost.

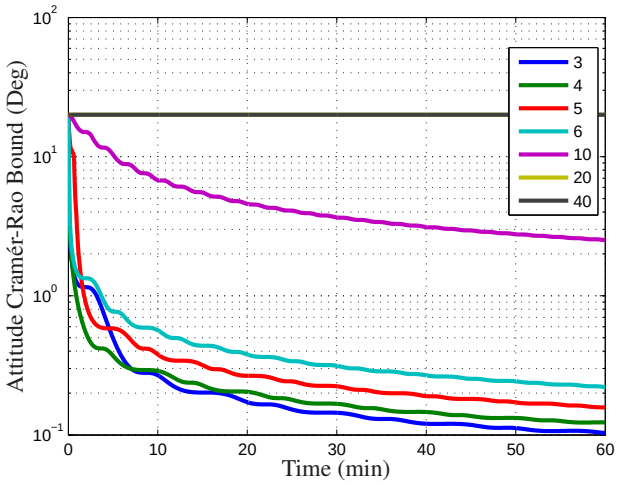

Figure 6. Test Case Cramér-Rao Lower Bound

CONCLUSION

In this paper, the Fisher information matrix and Cramér-Rao lower bound are introduced for calculating the observability of parameters used in Space Object (SO) models. The models used for photometric and astrometric data fusion were also introduced. Faceted shape models are discussed and the shape model geometry was introduced. The bi-directional distribution function models were

summarized and its partial calculation are given. An illustrative two-dimensional example was first considered. This example consisted of just one angle and one angle rate in the estimation problem. Using the Cramér-Rao lower bound the effects of geometry on estimation performance was studied. It was found that as the number of sides increases the SO tends to a axially symmetric object and the observability in the attitude estimation process is lost.

REFERENCES

[1] Abercromby, K. J., Seitzer, P., Rodriguez, H. M., Barker, E. S., and Matney, M. J., "Survey and Chase: A New Method of Observations for the Michigan Orbital DEbris Survey Telescope (MODEST)," *Acta Astronautica*, Vol. 65, 2009, pp. 103–111.

[2] Jorgensen, K. M., *Using Reflectance Spectroscopy to Determine Material Type of Orbital Debris*, Ph.D. thesis, University of Colorado, May 2000.

[3] Seitzer, P., Cowardin, H. M., Barker, E., Abercromby, K. J., Foreman, G., and Horstman, M., "Photometric Studies of Orbital Debris at GEO," *5th European Space Debris Conference*, Darmstadt, Germany, March–April 2009.

[4] Abercromby, K., Hamada, K., Guyote, M., Okada, J., and Barker, E., "Remote and Ground Truth Spectral Measurement Comparisons," *Proceedings of the Advanced Maui Optical and Space Surveillance Technologies Conference*, Maui, HI, Sept. 2007, Paper E42.

[5] Cowardin, H., Seitzer, P., Abercromby, K., Barker, E., and Schildknecht, T., "Characterization of Orbital Debris Photometric Properties Derived from Laboratory-Based Measurements," *Proceedings of the Advanced Maui Optical and Space Surveillance Technologies Conference*, Maui, HI, Sept. 2010.

[6] Cowardin, H., Abercromby, K., Barker, E., Seitzer, P., Mulrooney, M., and Schildknecht, T., "An Assessment of GEO Orbital Debris Photometric Properties Derived from Laboratory-Based Measurements," *Proceedings of the Advanced Maui Optical and Space Surveillance Technologies Conference*, Maui, HI, Sept. 2009, Paper E25.

[7] Bush, K. A., Crockett, G. A., and Barnard, C., "Satellite discrimination from active and passive polarization signatures: simulation predictions using the TASAT satellite model," *SPIE*, Vol. 4481, 2002, pp. 46–57.

[8] Jah, M. and Madler, R., "Satellite Characterization: Angles and Light Curve Data Fusion for Spacecraft State and Parameter Estimation," *Proceedings of the Advanced Maui Optical and Space Surveillance Technologies Conference*, Vol. 49, Wailea, Maui, HI, Sept. 2007, Paper E49.

[9] Linares, R., Jah, M. K., and Crassidis, J. L., "Inactive Space Object Shape Estimation via Astrometric And Photometric Data Fusion," .

[10] Linares, R., Jah, M. K., and Crassidis, J. L., "Space Object Area-To-Mass Ratio Estimation Using Multiple Model Approaches," *Advances in the Astronautical Sciences*, Vol. 144, 2012, pp. 55–72.

[11] Linares, R., Jah, M. K., Crassidis, J. L., Leve, F. A., and Kelecy, T., "Astrometric and Photometric Data Fusion for Inactive Space Object Feature Estimation," *Proceedings of 62nd International Astronautical Congress, International Astronautical Federation*, Vol. 3, 2011, pp. 2289–2305.

[12] Linares, R., Leve, F. A., Jan, M. K., and Crassidis, J. L., "Space Object Mass-Specific Inertia Matrix Estimation From Photometric Data," *Advances in the Astronautical Sciences*, Vol. 144, 2012, pp. 41–54.

[13] Crassidis, J. L. and Junkins, J. L., *Optimal estimation of dynamic systems, Second edition*, CRC press, 2011.

[14] Ashikmin, M. and Shirley, P., "An Anisotropic Phong Light Reflection Model," Tech. Rep. UUCS-00-014, University of Utah, Salt Lake City, UT, 2000.

[15] Blinn, J. F., "Models of Light Reflection for Computer Synthesized Pictures," *SIGGRAPH '77: Proceedings of the 4th Annual Conference on Computer Graphics and Interactive Techniques*, San Jose, CA, June 1977, pp. 192–198.

[16] Cook, R. L. and Torrance, K. E., "A Reflectance Model for Computer Graphics," *ACM Transactions on Graphics*, Vol. 1, No. 1, Jan. 1982, pp. 7–24.

[17] Shuster, M. D., "Maximum Likelihood Estimation of Spacecraft Attitude," *The Journal of the Astronautical Sciences*, Vol. 37, No. 1, Jan.-March 1989, pp. 79–88.

[18] Hinks, J. C., Linares, R., and Crassidis, J. L., "Attitude Observability from Light Curve Measurements," *AIAA Guidance, Navigation, and Control (GNC) Conference*, No. 10.2514/6.2013-5005, AIAA, Boston, MA, 2013.